JOURNAL OF PROPULSION AND POWER
Vol. 24, No. 3, May–June 2008

Microphysical Modeling of Ground-Level Aircraft-Emitted Aerosol Formation: Roles of Sulfur-Containing Species

Hsi-Wu Wong,* Paul E. Yelvington,† Michael T. Timko,‡ Timothy B. Onasch,§ and Richard C. Miake-Lye¶
Aerodyne Research, Inc., Billerica, Massachusetts 01821
and
Jianye Zhang** and Ian A. Waitz††
Massachusetts Institute of Technology, Cambridge, Massachusetts 02139

DOI: 10.2514/1.32293

Particulate matter emissions from aircraft engines have received increased attention due to their impacts on climate, health, and regional air quality. However, understanding of particulate matter formation from aircraft emissions at ground level is still limited. In this work, a detailed, one-dimensional model consisting of plume chemistry, wake dilution, and aerosol microphysics was developed to study sulfur-containing aerosol formation in near-field aircraft plumes at ground level. Parametric studies of ambient conditions and engine operating parameters were performed following the centerline plume trajectories up to 1 km downstream. The sampling system used in a recent experimental measurement campaign (NASA APEX-1) was also investigated. Our results show that binary homogeneous nucleation of H_2SO_4–H_2O is sensitive to ambient conditions, and heterogeneous condensation on soot is dependent on engine power. The results also suggest that at certain atmospheric conditions the observations from the experimental sampling system at moderate (e.g., 30 m) downstream locations may not represent the particle evolution further downstream. A comparison with experimental data provided a limited initial assessment of the model. This assessment suggests that the important physics are being captured, and the model may be used to interpret experimental results and help guide future directions of field measurements.

Nomenclature

$B_{i,j}$	=	coagulation kernel between soot particles in the ith size bin and droplets in the jth size bin
$b(x)$	=	radius where the local properties are $1/e$ of the centerline values at x
C_a	=	concentration of H_2SO_4
C_L, C_{jk}	=	coflowing jet model constants
C_s	=	concentration of SO_3
$\bar{c}$	=	mean particle thermal speed
c_i, c_j	=	speeds of particles i and j
$\bar{D}$	=	average diffusivity
D_i, D_j	=	diffusivities of particles i and j
D_v	=	diffusivity of water vapor
$\bar{d}$	=	average diameter
d_i, d_j	=	diameters of volatile particles i and j
$d_{p,i}$	=	diameter of soot particles in the ith size bin
$f_{\mathrm{CL}}(x)$	=	plume centerline exhaust gas fraction at x
G_i	=	collision factor between aerosols and soot particles in the ith size bin
I_c, I_m, I_{qc}	=	coflowing jet integral constants
K_{ij}	=	Brownian coagulation kernel between particles i and j
k	=	coflowing jet spread constant
M_{e0}	=	initial excess momentum rate per unit density
$M_{w,a}$	=	molecular weight of H_2SO_4
$M_{w,i}$	=	molecular weight of species i
$M_{w,s}$	=	molecular weight of SO_3
m_i	=	condensed mass on soot particles in the ith size bin
N_i	=	number density of droplets in the ith size bin
N_0	=	Avogadro's number
n_i	=	concentration of embryos with i acid molecules or droplets in the ith size bin
$P_{a,j}$	=	partial pressure of volatile particle j
P_v	=	vapor pressure of water
$P_{a,j}^{\infty}$	=	saturation vapor pressure of volatile particle j
P_v^{∞}	=	saturation vapor pressure of water
r	=	radial distance from the centerline of a plume
T_a	=	ambient total temperature
$T_{\mathrm{CL}}(x)$	=	plume centerline static temperature at x
T_0	=	initial exhaust total temperature
t	=	time
u_a	=	coflow velocity
$u_{\mathrm{CL}}(x)$	=	plume centerline velocity at x
u_0	=	initial jet velocity
$X_{\mathrm{amb},i}$	=	ambient mass fraction of gas-phase species i or ambient concentration of particulate species i
X_i	=	mass fraction of gas-phase species i, concentration of volatile particle i, or condensed mass on soot particles in the ith size bin
x	=	axial distance downstream of engine exit
α_d	=	mass accommodation coefficient of SO_3 or H_2SO_4 on unactivated (uncoated) soot surface
α_w	=	mass accommodation coefficient of volatile particles on activated (coated) soot surface
β_i	=	condensation rate of embryos with i acid molecules
γ_i	=	evaporation rate of embryos with i acid molecules

Received 25 May 2007; revision received 26 November 2007; accepted for publication 15 December 2007.

*Senior Engineer, Center for Aerothermodynamics, 45 Manning Road.
†Principle Engineer, Center for Aerothermodynamics, 45 Manning Road.
‡Senior Engineer, Center for Aerothermodynamics, 45 Manning Road.
§Principle Scientist, Center for Aerosol Cloud Chemistry, 45 Manning Road.
¶Principle Scientist and Director, Center for Aerothermodynamics, Vice President, 45 Manning Road.
**Graduate Student, Department of Aeronautics and Astronautics.
††Jerome C. Hunsaker Professor and Head, Department of Aeronautics and Astronautics. Fellow AIAA.

$\bar{\delta}$ = mean free distance
ε = fuel sulfur conversion factor
θ_i = activated (coated) fraction of surface for soot particles in the ith size bin
κ = Kelvin factor
λ = molecular mean free path in air
ρ_{pl} = plume density
σ_0 = average number of sites (molecules) per unit area of soot surface
$\dot{\omega}_i$ = overall chemical molar reaction rate of species i

I. Introduction

AIRCRAFT emissions have received growing attention during the past few years due to the increase of commercial traffic and heightened global environmental awareness. Particulate matter (PM) emissions composed of solid particles, volatile aerosols, and solid particles coated with condensable liquid in near-field aircraft plumes are of particular interest, because very fine aerosols (less than 2.5 μm in diameter) are known to provide risks to human health and also to affect the atmospheric processes that influence global climate change. Because of their potential impacts on climate, health, and regional air quality [1,2], it is necessary to understand how these aerosols are formed and how they may be managed.

Many studies have been performed to characterize particulate emissions from aircraft engines. Recent field measurements, such as the aircraft particle emission experiment series (APEX-1, JETS/APEX-2, and APEX-3 [3,4]), have been conducted to examine both gaseous and particulate emissions from commercial aircraft engines at ground level. These measurements show that chemical compositions and particle size distributions of aircraft-emitted, volatile aerosols are sensitive to sampling system design and operation, atmospheric conditions, and engine operating parameters. As a result, repeatable and accurate measurements are challenging because some important factors (such as ambient temperature and relative humidity) cannot be controlled in the experiment. Furthermore, understanding of aerosol microphysical processes such as particle nucleation, coagulation, growth, and condensation in near-field aircraft plumes at ground level is still limited. Therefore, it is important to gain an improved understanding of the effects of ambient conditions and engine operating parameters on the formation of aircraft-emitted aerosols.

Detailed microphysical modeling provides a useful way to understand aerosol formation mechanisms in near-field aircraft plumes. Previous efforts to model aircraft particulate matter emissions mostly focused on particles formed at high altitudes under cruise conditions [5–16]. Under these conditions, where ambient temperature and pressure are much lower than those at ground level (nominally 219 K and 0.24 atm at cruise conditions), the nucleation of the volatile particles was found to be extremely rapid, such that the volatile particles are nucleated 20 m downstream from the engine-exit plane within 0.1 s. At cruise, the particle growth was driven by water vapor freezing onto ice-coated particles during contrail formation. Because of the rapid temperature drop in the plume and the large supersaturation of water vapor with respect to ice, significant growth of both volatile and nonvolatile aerosols was predicted. However, these observations are not generally true for the ground-level aircraft emissions, where ambient conditions and engine operating parameters are significantly different. Several studies of particulate emissions from automobile diesel engines [17–22] have shown that aerosol growth is dependent on the ambient air dilution history and is sensitive to ambient conditions such as temperature and relative humidity. Although aircraft-emitted aerosols at high altitude and automobile-emitted aerosols at ground level have been studied via modeling, relatively few efforts have focused on the modeling of aerosol formation in near-field aircraft plumes at ground level. In the modeling study by Vancassel et al. [23], the particle growth was concluded to be enhanced when soot particle size decreases. However, understanding of the underlying particle growth mechanism is still lacking. In addition, there is a need to better understand the sensitivity of aerosol formation and chemical composition to ambient conditions and engine operating parameters under ground-level conditions. A reliable model may be used to interpret measurement results under various experimental conditions and to provide guidance for future aircraft emission measurement campaigns.

In this paper, a detailed one-dimensional microphysical model is presented to study the aerosol formation microphysics in near-field aircraft plumes at ground level. We have focused our work on the microphysical processes of the H_2SO_4–H_2O binary system as the first step of investigation and do not explicitly consider the effects of ion-induced or organics-enhanced nucleation processes. To provide local thermal conditions, initial exhaust properties were calculated, and a semi-empirical approach was used to estimate the plume dilution history. Parametric studies of ambient conditions and engine operating parameters were performed, and the effects of these parameters on the formation of aircraft-emitted aerosols are discussed.

II. Model Development

A. Determination of Initial Exhaust Properties

The first task required to model the microphysics of aerosol formation in near-field aircraft plumes is to estimate exhaust properties at the engine-exit plane. In this work, we have only focused on the CFM56-2C1 engines examined during the APEX-1 measurement campaign [3,4]. GasTurb, a gas-turbine cycle simulation program developed by Kurzke [24], was used to determine engine performance for different ambient conditions and engine operating parameters. A generic two-spool, unmixed-flow, turbofan engine configuration was chosen to model CFM56-2C1 engines. Engine design parameters, such as thrust settings, bypass ratio, overall pressure ratio, and mass flow rates of the core and the bypass, were gathered from *Jane's All the World's Aircraft* [25] when available, and the fuel flow rates at various power settings were taken from the International Civil Aviation Organization (ICAO) Emission Databank [26]. Based on these parameters, temperature, pressure, and velocity were calculated at various engine stations, including the engine-exit plane.

The initial concentrations of the gas-phase species at the engine-exit plane were calculated using a two-step equilibrium process [27] using the temperature and pressure values determined from the engine cycle calculations described previously. In the first step, the gas-phase species were assumed to be in equilibrium in the combustor. The combustor inlet concentrations were estimated based on the fuel-to-air ratio, and the C/H ratio and heating value of butene (C_4H_8) were used to represent fuel properties in this calculation. The calculated species concentrations from this step were then used as initial conditions at the turbine inlet for the second step. In the second step, the majority of the gas-phase species were assumed to be in equilibrium at the turbine exit. However, concentrations of species that are known not to be in equilibrium were fixed at the levels reported in the ICAO database (CO and NO_x) or estimated according to the fuel composition (SO_x). The constrained equilibrium calculation assumes that most combustion reactions take place very rapidly and chemical species are controlled by their thermodynamic states. This assumption was found to be able to produce reasonable results [27], and the technique of constrained equilibrium calculation was used to obtain initial concentrations of the gas-phase species at the engine-exit plane in this work.

B. Modeling of Plume Dilution History

In addition to engine-exit plane exhaust properties, dilution behavior of near-field aircraft plumes was also needed. In this work, plume temperature, velocity, and exhaust gas fraction as a function of downstream distance provided the time-varying thermal state for the one-dimensional microphysical model to follow. The semi-empirical, self-similar approach developed by Davidson and Wang [28] was used to estimate the plume dilution history instead of a full

flowfield analysis. Although the Davidson–Wang model does not capture the whole flowfield properties in detail as computational fluid dynamics (CFD) methods, it provides a fast and simple way to provide necessary flowfield information for our microphysical simulations. We have included the detail description of the Davidson–Wang algorithm in the Appendix section.

Figure 1 shows a comparison of predicted and measured values of velocity (Fig. 1a), temperature (Fig. 1b), and exhaust gas fraction (Fig. 1c) in near-field aircraft plumes at 30 m downstream as a function of engine power for CFM56-2C1 engines. Four different radial locations (centerline, 1, 2, and 3 m) at 30 m downstream were calculated from the Davidson–Wang model at an ambient temperature of 300 K and relative humidity of 10%. These conditions were chosen to approximate APEX-1 conditions, where the ambient temperature ranged from 290 to 310 K, and the ambient relative humidity ranged from 7 to 17%. Figure 1 shows that model predictions of the centerline properties were generally higher than the experimental values. This discrepancy is most likely due to the fact that the model does not account for varying of wind directions or location offsets during measurements. In fact, the measured values were best matched to the model prediction of 2 m off the centerline. Although there are uncertainties in both modeling and measurements that could account for the deviations observed, the results in Fig. 1 show that the Davidson–Wang model adequately captures the plume dilution behavior. However, to understand the mixing behavior of aircraft exhaust with ambient air in more detail, further investigation of plume dilution behavior using CFD is necessary to resolve several issues with mixing in near-field aircraft plumes, including how the potential core should be handled in the model and how well the two-stream, semi-empirical model used here can represent the complex turbulent flow system of a near-field jet engine plume.

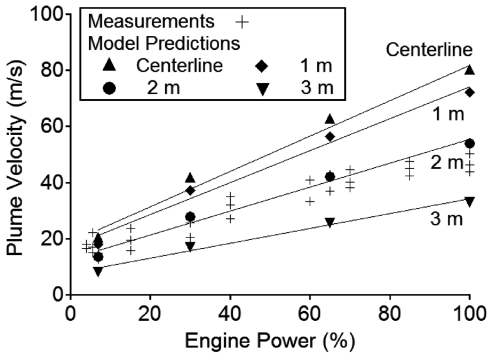

a) Plume velocity

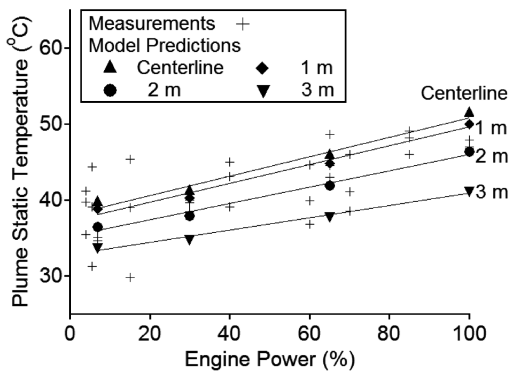

b) Plume static temperature

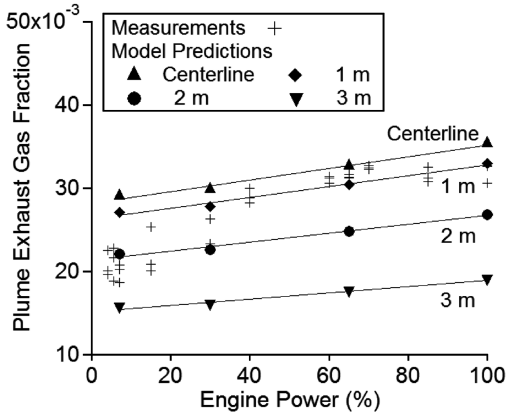

c) Plume exhaust mass fraction

Fig. 1 Comparison of predicted and measured properties in near-field aircraft plumes at 30 m downstream.

C. Detailed One-Dimensional Microphysical Model

In the one-dimensional microphysical model presented in this work, the time evolution of any gaseous or particulate species in a jet engine exhaust after the engine-exit plane is described as [11]

$$\frac{\mathrm{d}X_i}{\mathrm{d}t} = \left.\frac{\mathrm{d}X_i}{\mathrm{d}t}\right|_{\text{chemistry}} + \left.\frac{\mathrm{d}X_i}{\mathrm{d}t}\right|_{\text{mixing}} + \left.\frac{\mathrm{d}X_i}{\mathrm{d}t}\right|_{\text{microphysics}} \tag{1}$$

In our model, both liquid aerosols and coated black carbon soot particles are assumed to be perfectly spherical. The three terms on the right-hand side (RHS) of Eq. (1) correspond to the rates of production or disappearance from chemical reactions, wake dilution and mixing, and microphysical processes, respectively.

To evaluate the contribution from chemical reactions, the first term on the RHS of Eq. (1) is written as

$$\left.\frac{\mathrm{d}X_i}{\mathrm{d}t}\right|_{\text{chemistry}} = M_{w,i} \cdot \dot{\omega}_i \cdot \frac{1}{\rho_{\text{pl}}} \tag{2}$$

where $M_{w,i}$ is the molecular weight of species i, $\dot{\omega}_i$ is the overall molar chemical reaction rate (positive for production and negative for disappearance) of species i, and ρ_{pl} is the plume density. Equation (2) applies to the gaseous species only, because particulate species do not participate in any of the chemical reactions in our model. A gas-phase reaction mechanism containing 35 chemical species and 181 chemical reactions derived from the NO_x and SO_x combustion mechanism by Mueller et al. [29] was used in this work, and molar production rates were evaluated by CHEMKIN subroutines [30]. Additionally, the rate constants for forming sulfuric acid (H_2SO_4) from reacting water with SO_3 were taken from our previous study [6].

The contribution of wake dilution and mixing in Eq. (1) is written as

$$\left.\frac{\mathrm{d}X_i}{\mathrm{d}t}\right|_{\text{mixing}} = (X_i - X_{\text{amb},i}) \cdot \frac{\mathrm{d}f(t)}{\mathrm{d}t} \cdot \frac{1}{f(t)} \tag{3}$$

where $f(t)$ explains how the plume is diluted by the ambient air and can be derived from the exhaust gas fraction calculated using the Davidson–Wang algorithm. Note that $\mathrm{d}X_i/\mathrm{d}t|_{\text{mixing}}$ is equal to zero for condensed mass on soot because it is a surface, rather than bulk gas, property.

The third term on the RHS of Eq. (1) describes the contribution of microphysical processes and is further divided into three elements:

$$\left.\frac{\mathrm{d}X_i}{\mathrm{d}t}\right|_{\text{microphysics}} = \left.\frac{\mathrm{d}X_i}{\mathrm{d}t}\right|_{\text{nucleation}} + \left.\frac{\mathrm{d}X_i}{\mathrm{d}t}\right|_{\text{coagulation}} + \left.\frac{\mathrm{d}X_i}{\mathrm{d}t}\right|_{\text{soot}} \tag{4}$$

where the first term on the RHS of Eq. (4) describes the binary homogeneous nucleation of sulfuric acid (H_2SO_4) and water (H_2O), the second term describes the coagulation of liquid embryos and droplets, and the third term describes the microphysical processes taking place on the soot particle surface.

Nucleation rates of H_2SO_4–H_2O embryos were evaluated using the kinetic quasi-unary nucleation (KQUN) theory [31,32] as a more

accurate alternative to classical nucleation theory in this work. KQUN theory asserts that sulfuric acid nucleation kinetics is the controlling factor and that water reaches equilibrium with embryos and droplets immediately. This permits binary nucleation of H_2SO_4–H_2O to be treated as unary nucleation of sulfuric acid. The embryo formation rates due to homogeneous binary nucleation are derived explicitly from the condensation and evaporation rates:

$$\frac{dn_i}{dt} = \beta_{i-1}n_{i-1} - \gamma_i n_i - \beta_i n_i + \gamma_{i+1}n_{i+1} \qquad (i > 2) \qquad (5a)$$

$$\frac{dn_2}{dt} = \frac{1}{2}\beta_1 n_1 - \gamma_2 n_2 - \beta_2 n_2 + \gamma_3 n_3 \qquad (i = 2) \qquad (5b)$$

$$\frac{dn_1}{dt} = 2\gamma_2 n_2 + \sum_{i=3}^{m}\gamma_i n_i - \sum_{1}^{m-1}\beta_i n_i \qquad (i = 1) \qquad (5c)$$

In Eq. (5), m is a user-specified value representing the size of the largest embryo tracked in the model. Compared with classical binary homogeneous nucleation theory of H_2SO_4–H_2O cluster formation, this kinetic based theory has the advantage of capturing particle distributions in a rapidly diluting engine exhaust where dramatic changes in temperature, relative humidity, and sulfuric acid concentration take place [22].

The second term on the RHS of Eq. (4) corresponds to the coagulation of different liquid particles. This term includes the condensational growth of sulfuric acid monomer on H_2SO_4–H_2O embryos or droplets, which is written as [33]

$$\frac{dn_k}{dt} = \frac{1}{2}\sum_{i+j=k} K_{ii}n_i n_j - \sum_{i=1}^{l} K_{ik}n_i n_k \qquad (6)$$

where the Brownian coagulation kernel K_{ij} is evaluated as [34]

$$K_{ij}(d_i, d_j) = \frac{8\pi\bar{d}\bar{D}}{\bar{d}/(\bar{d}+\bar{\delta}) + 4\bar{D}/(\bar{d}+\bar{c})} \qquad (7)$$

in which $\bar{d} = (d_i + d_j)/2$, $\bar{D} = (D_i + D_j)/2$, $\bar{c} = (c_i^2 + c_j^2)^{1/2}$, and $\bar{\delta} = (\delta_i^2 + \delta_j^2)^{1/2}$.

When Eq. (6) applies to the embryos included in Eq. (5), i, j, k, and l denote the size of the embryos and are no bigger than m, which is the size of the largest embryo included in Eq. (5). Because tracking the exact composition of large particles is impractical, the fully stationary sectional bin approach [35] was used to track droplets that are beyond the largest embryo specified. In this case, l denotes the total number of sectional bins, which is a user-specified value. Mass conservation was taken into account across the boundary between the embryos and the binned particles.

The first and second terms on the RHS of Eq. (6) correspond to the formation and disappearance of aerosol droplets, respectively. Because quasi-unary nucleation theory explicitly considers sulfuric acid condensing on or evaporating from embryos, the condensational growth in Eq. (6) does not apply to the H_2SO_4–H_2O embryos governed by Eq. (5). The amount of water change from coagulation is also calculated based on the equilibrium compositions of different particle sizes.

The third term on the RHS of Eq. (4) describes the microphysical interactions between nucleated H_2SO_4–H_2O aerosols and the soot particles. The size evolution of soot particles is expressed as the combination of soot activation and condensational growth [11]:

$$\frac{dm_i}{dt} = \left.\frac{dm_i}{dt}\right|_{\text{activation}} + \left.\frac{dm_i}{dt}\right|_{\text{condensation}} \qquad (8)$$

The soot activation is further divided into adsorption and scavenging:

$$\left.\frac{dm_i}{dt}\right|_{\text{activation}} = \left.\frac{dm_i}{dt}\right|_{\text{adsorp.}} + \left.\frac{dm_i}{dt}\right|_{\text{scav.}} \qquad (9)$$

where adsorption is achieved by H_2SO_4 and its precursor SO_3 as

$$\left.\frac{dm_i}{dt}\right|_{\text{adsorp.}} = \frac{1}{4}\cdot\alpha_d\cdot\bar{c}\cdot d_{p,i}^2\cdot(1-\theta_i)\cdot(C_s M_{w,s} + C_a M_{w,a}) \qquad (10)$$

in which α_d was set to be 0.018 in accordance with recent laboratory findings [36].

The scavenging of H_2SO_4–H_2O embryos and droplets is written as

$$\left.\frac{dm_i}{dt}\right|_{\text{scav}} = \frac{1}{4}\cdot\pi\cdot\sum_j B_{i,j}N_j\left[\frac{d_j}{d_{p,i}}\right]^2(1-\theta_i)\cdot M_{w,j} \qquad (11)$$

As shown in Eqs. (10) and (11), the activation and scavenging rates are linearly dependent on the unactivated (uncoated) fraction of the soot particle surfaces $1-\theta_i$, and θ_i is described by

$$\frac{d\theta_i}{dt} = \left.\frac{d\theta_i}{dt}\right|_{\text{adsorp.}} + \left.\frac{d\theta_i}{dt}\right|_{\text{scav.}} \qquad (12)$$

$$\left.\frac{d\theta_i}{dt}\right|_{\text{adsorp.}} = \frac{1}{4}\cdot\alpha\cdot\bar{c}\cdot\frac{N_0}{\sigma_0}\cdot(1-\theta_i)\cdot(C_s + C_a) \qquad (13)$$

$$\left.\frac{d\theta_i}{dt}\right|_{\text{scav}} = \frac{1}{4}\cdot\pi\cdot\sum_j B_{i,j}N_j\left[\frac{d_{p,j}}{d_{p,i}}\right]^2(1-\theta_i) \qquad (14)$$

where σ_0 is set at 5×10^{18} m^{-2} [11].

The growth on soot particles is broken into contributions from condensation of both sulfur-containing aerosols and water vapor:

$$\left.\frac{dm_i}{dt}\right|_{\text{condensation}} = \left.\frac{dm_i}{dt}\right|_{\text{sulfur}} + \left.\frac{dm_i}{dt}\right|_{\text{water}} \qquad (15)$$

in which

$$\left.\frac{dm_i}{dt}\right|_{\text{sulfur}} = 2\pi G_i N_0\sum_j\left[D_j d_{p,i}\theta_i\left(\frac{P_{a,j} - \kappa P_{a,j}^{\infty}}{RT}\right)\cdot M_{w,j}\right] \qquad (16)$$

$$\left.\frac{dm_i}{dt}\right|_{\text{water}} = 2\pi G_i N_0 D_v d_{p,i}\theta_i\left(\frac{P_v - \kappa P_v^{\infty}}{RT}\right)\cdot M_{w,v} \qquad (17)$$

and G_i is expressed as [37]

$$G_i = \left[\frac{1}{1+\frac{2\lambda}{d_{p,i}}} + \frac{2\lambda}{3\alpha_w d_{p,i}}\right]^{-1} \qquad (18)$$

where α_w is set at unity for both water vapor and sulfur-containing aerosol condensation on coated soot particles [11].

In Eq. (16), the sulfur-containing liquid embryos and droplets of all sizes contribute to the condensational growth of soot particles. For sulfuric acid monomers, the pressure difference term $P_{a,j} - P_{a,j}^{\infty}$ is present, because sulfuric acid monomers have noticeable vapor pressure under the conditions of interest and can evaporate from coated soot surfaces. For other larger embryos or droplets, $P_{a,j}^{\infty}$ is assumed to be zero and the pressure difference terms are reduced to the partial pressure of the condensing aerosol species because these aerosols have very low saturation vapor pressure under our conditions of interest.

The contributions of mixing and microphysical terms of Eq. (1) are generally more significant than the chemistry term under conditions of ground-level aircraft plumes, because oxidation reactions normally take place at higher temperatures and atmospheric reactions usually take place in slower rates. Far enough downstream of a plume where ambient dilution processes become much slower, the aerosol microphysical processes become more important especially at lower ambient temperatures. The relative importance of each microphysical term in Eq. (4) is dependent on ambient conditions and engine operating parameters. The homogeneous

nucleation and coagulation processes become more important at lower ambient temperature and higher level of relative humidity. This is because binary homogenous H_2SO_4–H_2O nucleation, coagulation, and particle growth are strongly dependent on ambient temperature and relative humidity. The soot microphysics is more significant at higher engine thrusts, where a larger amount of soot particles (and thus a larger soot surface area) is emitted from the aircraft. We will discuss these effects along with our modeling results in the next section.

III. Results and Discussion

Parametric studies of ambient conditions and engine operating parameters were performed to determine the formation mechanisms of H_2SO_4–H_2O aerosols in near-field aircraft plumes. Simulations were carried out at three different ambient temperatures (286, 293, and 300 K), four different levels of ambient relative humidity (10, 40, 60, and 80%), four different power settings (7, 30, 65, 100%), and two different fuel sulfur contents (FSC, 383 and 1595 ppm). In these runs, the fuel sulfur conversion factor (ε) to S^{VI} (sulfur with an oxidation state of +6) was assumed to be 1% [38], that is, S^{VI} mass is 1% of the total sulfur mass at the engine-exit plane. The remaining sulfur mass has an oxidation state of +4 (S^{IV}), which is primarily present in SO_2 and stays as S^{IV} during plume evolution because SO_2 oxidation takes place very slowly after the engine-exit plane where the temperature is significantly lower. The soot particles were initially log-normally distributed into 30 bins from 3 to 250 nm in diameter, and the parameters of the log-normal distribution were fitted into the experimental data gathered in APEX-1 for CFM56-2C1 engines [39,40], as listed in Table 1. The parameter space explored provides a comprehensive way to study the sensitivity of aircraft-emitted aerosol formation to these factors.

Several factors affect the accuracy of our model prediction. First, microphysics of ion-induced nucleation and organics-enhanced nucleation are both neglected in our model. Chemiions in the exhaust of aircraft jet engines have been measured in the literature [41–45]. It has been reported that chemiions may enhance the nucleation rates of the H_2SO_4–H_2O system, reducing the sensitivity of particle formation to ambient conditions [8,17,18]. However, detailed interactions between chemiions and H_2SO_4–H_2O droplets are very complicated [46,47], and knowledge of how chemiions affect the formation and growth of aircraft-emitted aerosols at ground level is still limited. Enhancement of nucleation rates by organics may also be critical [48]. This process may be more important at lower power settings where significantly more organic emissions are present in the gas and condensed phases [49,50]. However, the mechanisms for organics-enhanced nucleation are still unknown, as are the species involved and the process by which the organics contribute to the aerosol growth. Finally, the values for several model parameters, such as α_d and ε, are still uncertain in the literature and therefore could also affect the outcome of our model prediction. Although the modeling tool developed in this work may not capture all the microphysical details taking place in a near-field aircraft plume, the results still provide valuable information to understand the importance of the critical formation mechanisms of aircraft-emitted sulfur-containing aerosols at ground level. The results are also helpful for interpreting current measurement data.

In this work, the aerosol dynamics in near-field aircraft plumes following centerline trajectories up to 1 km downstream were simulated within the parameter space described previously. In addition, the particle formation mechanisms inside the APEX 30-m downstream sampling system were studied. The results of these calculations are discussed in the following sections.

A. Aerosol Dynamics in Near-Field Aircraft Plumes

1. Representative Simulation Results

Figure 2 shows a set of representative results from a one-dimensional microphysical simulation following an exhaust centerline trajectory up to 1 km downstream in a near-field aircraft plume. The ambient temperature was 286 K and the ambient relative humidity was 60%. The engine power was set at 7%, and the fuel sulfur content was 383 ppm. The growth of H_2SO_4–H_2O liquid particles was divided into two parts: the embryos (i.e., H_2SO_4–H_2O oligomers), which are particles smaller than or equal to a user-specified size set at 40 acid molecules, and the droplets, which are particles beyond the largest embryos tracked. The embryos were specifically tracked by their sizes, and the droplets were discretized into 30 log-normally distributed bins covering diameters up to 250 nm. The concentration evolution results for liquid $H_2SO_4 - H_2O$ droplets and embryos are shown in Figs. 2a and 2b, respectively. As shown in these figures, the geometric mean diameter of H_2SO_4–H_2O droplets reached about 27 nm at 1 km downstream (Fig. 2a), and the embryos served as nuclei of this particle growth (Fig. 2b). After 800 m downstream, which is at a plume age of about 9 min, the liquid particle growth almost reached equilibrium and the concentrations of the droplets started to decline because of the mixing of the plume with ambient air.

Figure 2c shows the evolution of soot particles, where the geometric mean diameter of the particles increased from 16 nm to about 28 nm at 1 km downstream. This particle growth was driven by the activation, scavenging, and condensation of SO_3, H_2SO_4, H_2O, and H_2SO_4–H_2O aerosols onto the soot particles, as described in Sec. II.C. The size distributions of soot particles shown here can be combined with the size distributions of liquid H_2SO_4–H_2O droplets in Fig. 2a. As shown in Fig. 2d, a bimodal distribution including both nucleation and soot modes was found in a near-field aircraft plume at 1 km downstream. In comparison with other modeling efforts of aircraft particulate matter emissions at high altitudes under cruise conditions [6,10,11,15], the particle growth at ground level predicted in this work is much slower and the resulting particle size is much smaller.

An instructive way to understand the growth of sulfur-containing aerosols in near-field aircraft plumes is to consider the evolution of the sulfur mass budget. In Fig. 2e, the S^{VI} mass budget is divided into three categories: 1) the S^{VI} mass in the vapor phase consisting of H_2SO_4–$(H_2O)_n$ monomers and its gas-phase precursors SO_3 and H_2SO_4; 2) the S^{VI} mass in aerosol droplets and embryos formed via binary H_2SO_4–H_2O nucleation; 3) the S^{VI} mass in soot coatings from the condensational growth on soot particles. As shown in Fig. 2e, the S^{VI} mass in the aerosol droplets and that in the soot coatings both increased with increasing downstream distance as nucleation and condensational growth occurred. At 1 km downstream, roughly 40 and 31% of the S^{VI} mass (0.4 and 0.31% of the total sulfur mass) was in the aerosol droplets and soot coatings, respectively, and around 28% of the S^{VI} mass (0.28% of the total sulfur mass) remained in the vapor phase. Based on this finding, the soot particles are likely to continue to grow further downstream, because nucleation had almost reached equilibrium, and both gas-phase SO_3 and H_2SO_4 and liquid-phase embryos and droplets would continue to condense on soot particles. However, it is also possible that sulfuric acid would be sufficiently diluted far enough downstream to reach its saturation

Table 1 The parameters used for log-normally distributed soot particles under different power settings

Power settings, %	Initial concentration, cm^{-3}	Geometric mean diameter, nm	Standard deviation	Estimated surface area, m^2/cm^3[a]
100	3.0×10^7	35.0	1.6	1.795×10^{-7}
65	7.5×10^6	25.0	1.6	2.291×10^{-8}
30	6.0×10^6	20.0	1.4	9.456×10^{-9}
7	8.5×10^6	16.0	1.3	7.845×10^{-9}

[a]Estimation was based on spherical particles log-normally distributed into 30 bins from 3 to 250 nm.

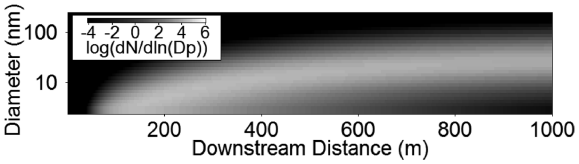

a) Concentration and size evolution of liquid droplets

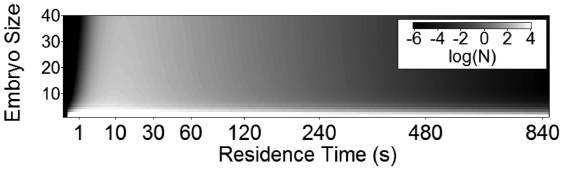

b) Concentration and size evolution of embryos

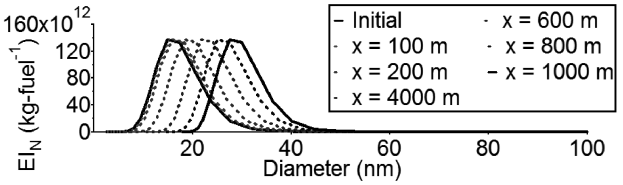

c) Size evolution of soot particles

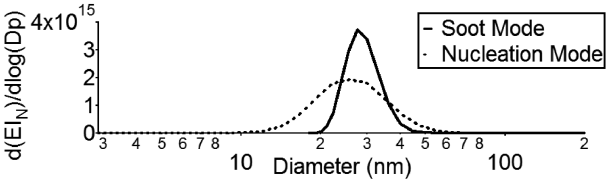

d) Final combined particle size distribution

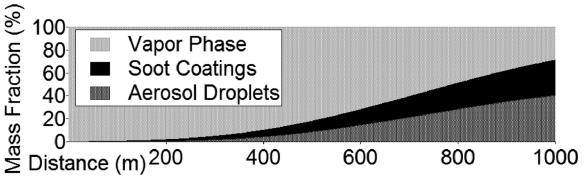

e) Evolution of S^{VI} mass fraction

Fig. 2 Representative simulation results following the plume centerline trajectory up to 1 km downstream.

vapor pressure. In this case, the equilibrium between condensation and evaporation of H_2SO_4 on coated soot particles is reached, and the S^{VI} mass in the vapor phase would no longer decline.

2. *Effects of Ambient Relative Humidity Levels and Engine Power Settings*

To study the sensitivity of H_2SO_4–H_2O aerosol formation to ambient conditions and engine operating parameters, the S^{VI} mass budget at 286 K under different levels of ambient relative humidity and engine power settings at 1 km downstream were examined. For direct comparison with experimental data, the S^{VI} mass budget was converted into the sulfate (SO_4) mass emission index (EI_m) as measured by the aerosol mass spectrometer (AMS) during APEX-1. Figure 3 shows the effects of engine power and ambient relative humidity on the sulfate EI_m at 1 km downstream under ambient temperature of 286 K and fuel sulfur content of 383 ppm. As shown in the figure, the contribution of the nucleation mode H_2SO_4–H_2O particles to the total sulfate mass increased sharply with increasing relative humidity. At 40 and 10% relative humidity (Figs. 3c and 3d), the homogeneous binary nucleation of H_2SO_4 and H_2O was found to be insignificant, and the sulfate mass emission index contribution from liquid H_2SO_4–H_2O aerosols was negligible under all power

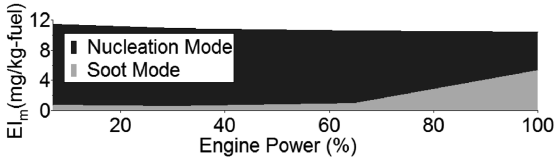

a) 80% relative humidity

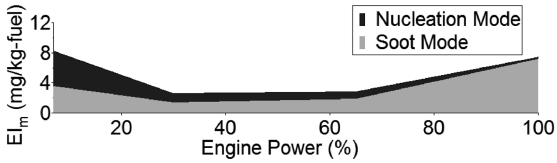

b) 60% relative humidity

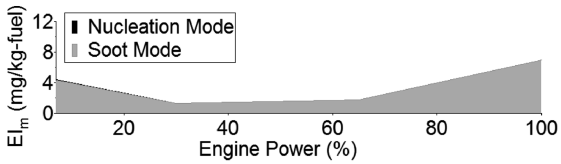

c) 40% relative humidity

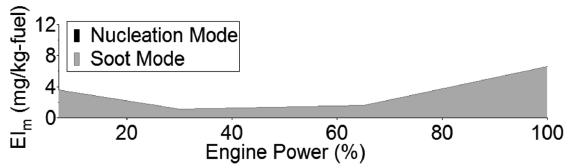

d) 10% relative humidity

Fig. 3 Effects of engine power and relative humidity on the sulfate EI_m at 1 km downstream.

settings. However, at 80% relative humidity (Fig. 3a), more than 5 mg/kg fuel of the total sulfate mass was contributed by liquid H_2SO_4–H_2O aerosols formed via binary nucleation of H_2SO_4 and H_2O under all power settings. This dependence of binary H_2SO_4–H_2O nucleation rates on relative humidity is due to the critical role that water plays in the nucleation process.

The sulfate mass emission index in the soot coatings (soot mode) is more correlated with the engine power settings. As shown in Fig. 3, the sulfate mass condensed on soot was the lowest under 30 and 65% engine power levels with a sulfate emission index of 1–2 mg/kg fuel. However, under 100 and 7% engine power, the sulfate emission index is significantly higher with more than 3.5 mg/kg fuel. This is because different initial size distributions of soot particles under different power settings were assigned, as listed in Table 1, and at high levels of engine power more soot surface area is available. This enables the condensation of gas-phase molecules or liquid aerosols more easily. This observation is consistent with the modeling study by Vancassel et al. [23]. On the other hand, more residence time is required for a plume generated at low levels of engine thrust to reach a given downstream distance, as illustrated in Fig. 4. For example, the plume age for 7% engine power was more than twice as long as the plume age for 30% engine power at 1 km downstream. A rapid increase in the plume age from 30 to 7% engine power resulted in an increase in sulfate mass condensed on soot particles because more time was available for condensation. This trend is the same under almost all levels of relative humidity. The only exception was at 80% relative humidity and 7% engine power, where the competition of the nucleation and condensation lowered the amount of sulfate mass condensed on soot particles.

An alternative way to present the results in Fig. 3 is to use a three-dimensional graph as shown in Fig. 5a. In this figure, the lower (light) plane represents the sulfate condensed on the soot particles (soot mode) and the upper (dark) plane represents the total sulfate consisting of both soot and nucleation modes. This graph is further

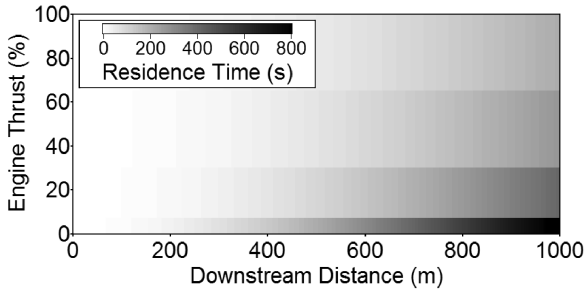

Fig. 4 The residence time and downstream distance of a plume as a function of engine thrust.

broken down into two contour plots in Figs. 5b and 5c, which describe the soot mode and the nucleation mode separately under different levels of relative humidity and power settings. Again, these figures show that the nucleation mode was very sensitive to ambient relative humidity so that the nucleation mode sulfate EI_m increased from being negligible at 10% relative humidity to about 10 mg/kg fuel at 80% relative humidity for 7–65% engine power settings. The soot mode was mainly dependent on engine power, and the soot mode sulfate EI_m ranged from 6 mg/kg fuel at 100% engine power to less than 2 mg/kg fuel at 65 or 30% engine power. As described earlier, there is a competition between the soot mode and the nucleation mode. This competition was found to be most marked in the upper right corners of the contour plots, where both the nucleation and soot modes are lower than their maximum emission index values. This is because both homogeneous nucleation and heterogeneous condensation deplete sulfuric acid and H_2SO_4–H_2O droplets and are both favored at high levels of relative humidity and engine power.

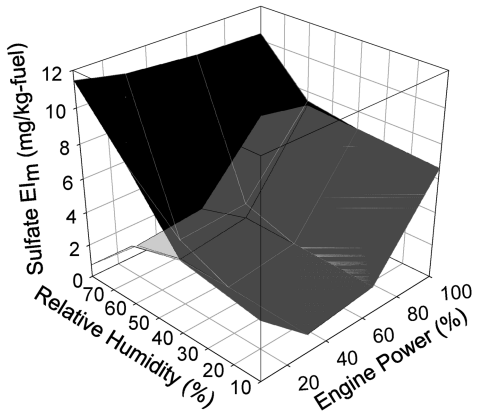

a) A 3-dimensional representation

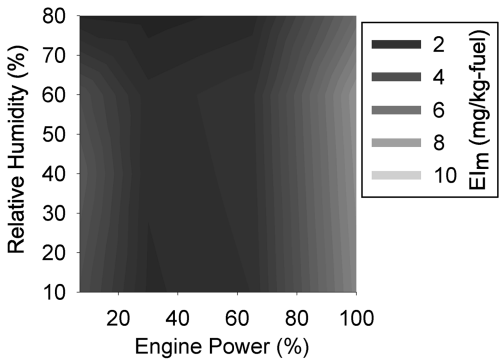

b) The soot mode sulfate EI_m

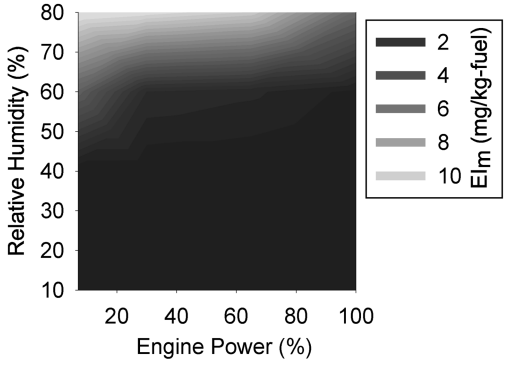

c) The nucleation mode sulfate EI_m

Fig. 5 The simulated sulfate EI_m at 1 km downstream.

3. Results for Plumes with Same Age and Effects of Ambient Temperature

To eliminate the effects of different plume ages on the amount of sulfate condensed on soot particles, the results were reanalyzed at a plume age of 3 min under different levels of ambient relative humidity and engine power to remove the effect of engine power on residence time. As shown in Fig. 6, the amount of the sulfate condensed on the soot increased with increasing engine power due to larger available soot surface area for the same plume age at an ambient temperature of 286 K. The soot mode sulfate EI_m at 7% engine power was significantly lower (~0.4 mg/kg fuel) in Fig. 6 compared to that in Fig. 5 (~4 mg/kg fuel) where a longer plume age was considered. The competition between the soot mode and the nucleation mode was also present and was most obvious at high relative humidity and high engine power conditions.

The effects of ambient temperature on particle formation at a plume age of 3 min under different levels of ambient relative humidity and engine power are shown in Fig. 7. The sensitivity of the nucleation mode sulfate to ambient temperature and relative humidity is clear from comparing Figs. 6 and 7. The nucleation mode sulfate EI_m increased with decreasing ambient temperature, ranging from 9 mg/kg fuel at 286 K to almost negligible at 300 K (at 80% relative humidity and 7% engine power). This sensitivity of the nucleation mode to ambient temperature and relative humidity predicted is consistent with what was simulated in the modeling study by Du and Yu [22] for automobile diesel engines. This observation also shows that it could be difficult to quantify the amount of sulfate mass in the homogeneous aerosol phase from experiments where ambient conditions are varying. On the other hand, the amount of the sulfate condensed on the soot was not sensitive to ambient conditions and was primarily dependent on engine power. The soot mode sulfate EI_m changed from 6 mg/kg fuel to 0.8 mg/kg fuel when engine power was reduced from 100 to 7%. The only exception was at 80% relative humidity, 100% engine power, and 286 K ambient temperature, where both homogeneous nucleation and heterogeneous condensation were favored. In this case, the competition of the two processes results in sensitivity of both nucleation and soot modes to ambient conditions and engine operation.

B. Aerosol Dynamics Inside the APEX 30-m Downstream Sampling System

1. Representative Simulation Results

To compare our modeling results with experimental findings, one-dimensional calculations reproducing the APEX-1 30-m downstream sampling system were performed. Figure 8 shows a set of representative results for these simulations under the same ambient conditions (ambient temperature of 286 K and ambient relative humidity of 60%) and engine operating parameters (engine power of 7% and fuel sulfur content of 383 ppm) as in Fig. 2. In these figures, the axial downstream distance was divided into two parts. The first 30 m of the calculations studied the microphysics that occur in the plume right after the engine-exit plane, and the

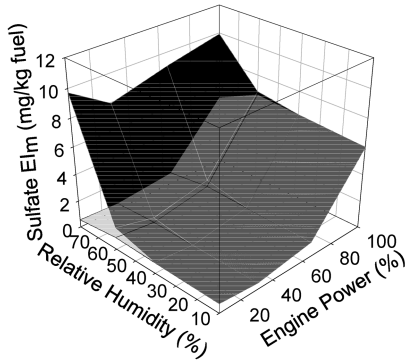

a) A 3-dimensional representation

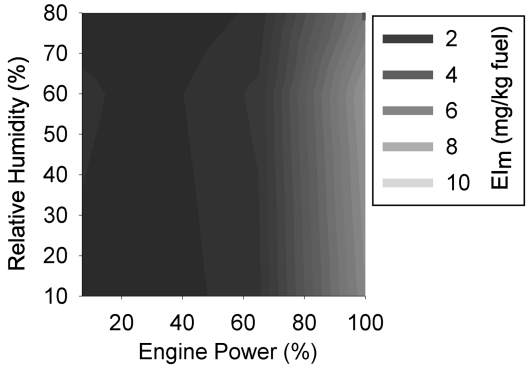

b) Contours for the soot mode sulfate EI_m

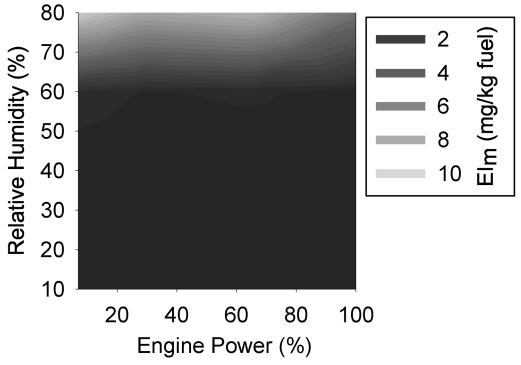

c) Contours for the nucleation mode sulfate EI_m

Fig. 6 The simulated sulfate EI_m at a plume age of 3 min at 286 K.

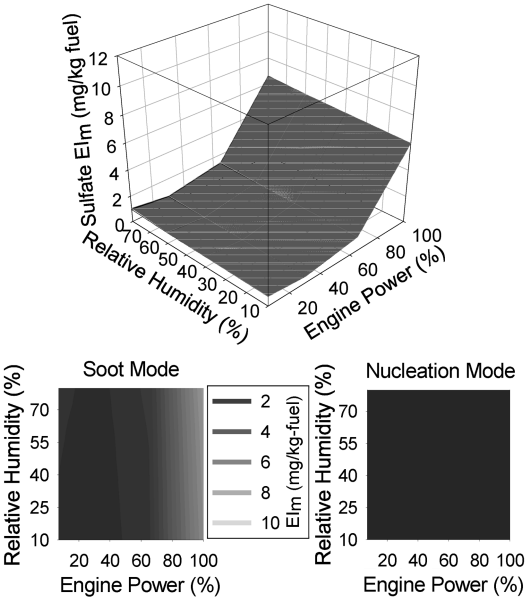

a) 293K

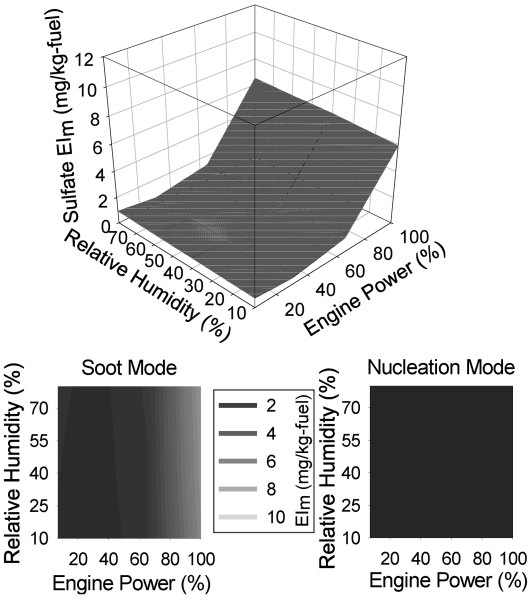

b) 300K

Fig. 7 The simulated sulfate EI_m at a plume age of 3 min.

remaining calculations simulated the microphysics that occur in the sampling system including both the probe tip and the sampling line. No additional dilution was permitted after the plume entered the sampling system, and the centerline velocity and temperature profiles in the sampling system were determined based on the measured values during APEX-1. As shown in Fig. 8, aerosol droplets and embryos bigger than 10 acid monomers did not start to form until the plume entered the sampling system. This is because the residence time required to travel from the engine-exit plane to the probe tip is too short (<0.85 s) and the plume centerline flow is too warm (>297.5 K) for binary homogeneous nucleation and condensation on soot particles to occur significantly. Further comparison of Figs. 2 and 8 reveals that the results for the 30-m sampling system do capture the microphysics of particle formation in the plume with the same plume age (~3 s) qualitatively well. However, the behavior of aerosol formation further downstream looks quite different both qualitatively and quantitatively from what was predicted for the 30-m sampling system. This suggests that residence time and exhaust dilution history have significant impacts on the aerosol formation microphysics.

2. *Effects of Ambient Conditions and Engine Operating Parameters*

Figure 9 shows the effects of ambient relative humidity, ambient temperature, and engine power on the formation of aerosol droplets and the growth of soot particles in the 30-m downstream sampling system. Similar to the findings of the near-field plume calculations, the binary homogeneous H_2SO_4–H_2O nucleation (nucleation mode) was very sensitive to the ambient conditions. The nucleation mode sulfate EI_m changed from negligible to about 6 mg/kg fuel when ambient relative humidity increased from 10 to 80% and ambient temperature decreased from 300 to 286 K. However, the sulfate mass condensed on soot particles (soot mode) was insensitive to ambient conditions and primarily dependent on engine power settings. The soot mode sulfate EI_m changed from 0.7 mg/kg fuel to 0.02 mg/kg fuel when engine power was lowered from 100 to 7%. Comparison of the results contained in Fig. 9 with Figs. 6 and 7 shows that the concentrations of the gas-phase H_2SO_4 and SO_3 in the sampling system were higher in this case, and the final nucleated or condensed sulfate mass was less due to a significantly shorter residence time. The competition between the soot mode and the

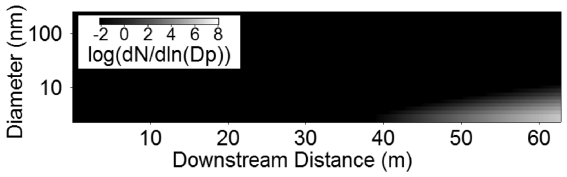

a) Concentration and size evolution of liquid droplets

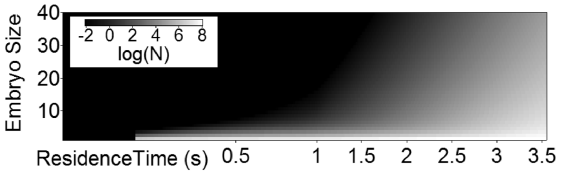

b) Concentration and size evolution of embryos

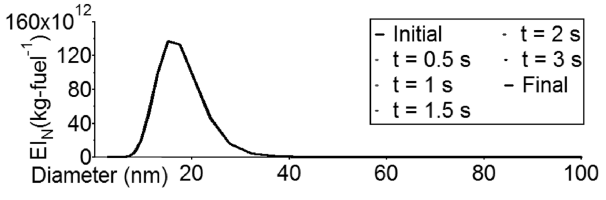

c) Size evolution of soot particles

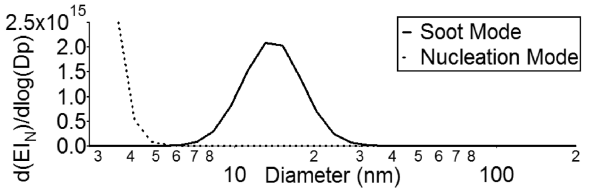

d) Final combined particle size distribution

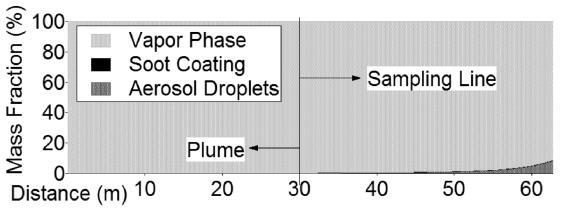

e) Evolution of S^{VI} mass fraction

Fig. 8 Representative simulation results in the APEX-1 30-m downstream sampling system.

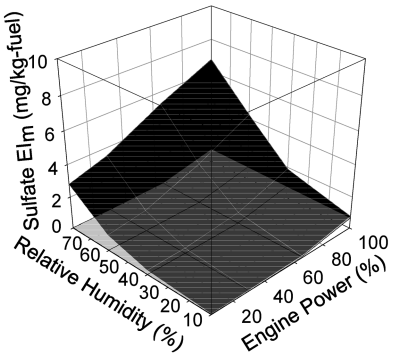

a) 286K

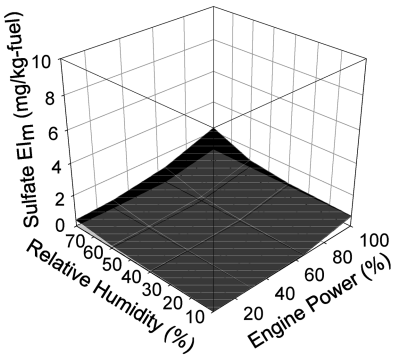

b) 293K

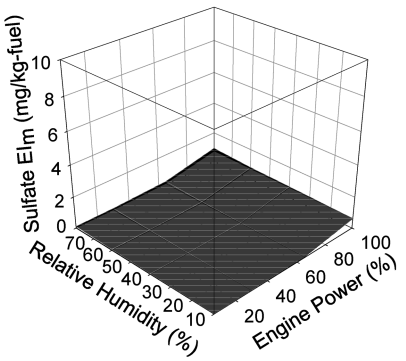

c) 300K

Fig. 9 The simulated sulfate EI_m in the APEX 30-m sampling system with a FSC of 383 ppm.

nucleation mode at 80% relative humidity, 100% engine power, and 286 K was also not as noticeable as what was found in the 3-min plume calculations.

The simulation results for the 30-m downstream sampling system with a fuel sulfur content of 1595 ppm are shown in Fig. 10. Similar to Fig. 9, the soot mode is engine power dependent, and the nucleation mode was sensitive to ambient temperature and relative humidity. The soot mode sulfate EI_m changed from 10 mg/kg fuel to 0.4 mg/kg fuel when engine power was decreased from 100 to 7%, and the nucleation mode sulfate EI_m changed from 0.06 mg/kg fuel to 38 mg/kg fuel when ambient relative humidity increased from 10 to 80% and ambient temperature decreased from 300 to 286 K. These results also show that the amount of sulfate in the nucleation increased with increasing FSC. According to these results, an increase of FSC from 383 to 1595 ppm resulted in an increase of total sulfate condensed on the soot particles of about 14-fold on average. Both homogeneous nucleation and heterogeneous condensation processes are more favorable when FSC is higher, and the competition between the soot mode and the nucleation mode is also more significant.

3. Comparison of Modeling Results and Experimental Data

In addition to the uncertainties embedded in the model described earlier, several difficulties related to field measurements make direct comparison between modeling results and experimental findings challenging. First, the minimum particle size that is sensed by the instruments usually complicates the comparison for the nucleation mode, because liquid droplets formed via homogeneous nucleation are mostly too small to be measured and quantified. This could potentially cause significant errors, especially when the signals are small. The fluctuations of the ambient conditions, such as temperature, relative humidity, and the wind direction affecting the dilution history may also play a big role due to the sensitivity of the nucleation mode to these parameters. Therefore, a direct comparison of the measured and the predicted nucleation mode sulfate EI_m is presently difficult. However, such a comparison can be performed for the sulfate mass condensed on soot particles, because this quantity is less affected by the factors described above. Figure 11 shows a comparison of the modeled and measured sulfate emission index for the soot mode as a function of engine power for both fuel sulfur contents (383, 1595 ppm). The modeling results were taken for the 30-m sampling system calculations at an ambient temperature of

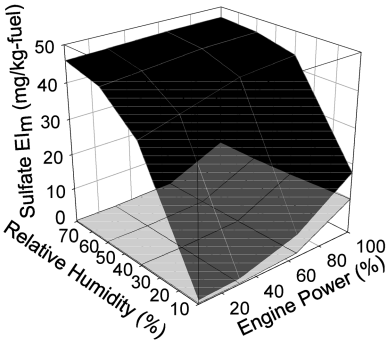

a) 286K

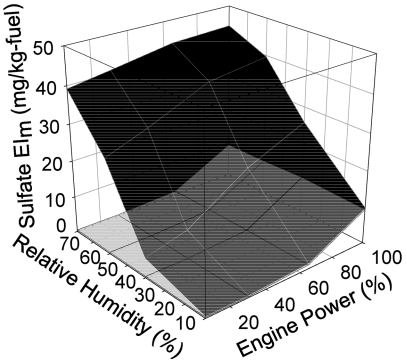

b) 293K

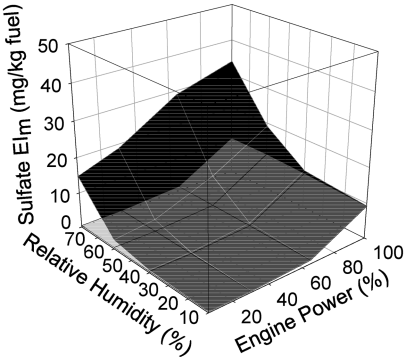

c) 300K

Fig. 10 The simulated sulfate EI_m in the APEX 30-m sampling system with a FSC of 1595 ppm.

300 K and ambient relative humidity of 10%. In addition to a 1% fuel sulfur conversion factor (ε), a set of simulation runs using a 2% fuel sulfur conversion factor under the same ambient conditions and engine operating parameters was also performed. The experimental

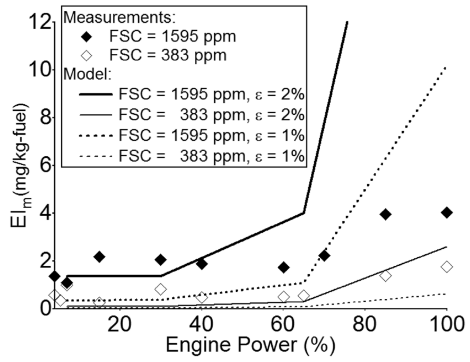

Fig. 11 Comparison of model-predicted and experimental [51] soot mode sulfate EI_m.

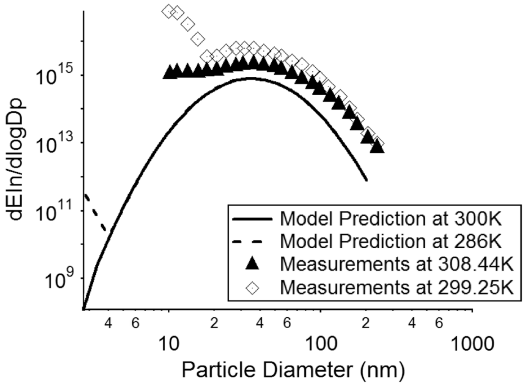

Fig. 12 Comparison of model-predicted and experimental [40] particle size distribution.

data were averaged from the AMS measurements for the 30-m downstream studies during the APEX-1 campaign [51], where the ambient temperature ranged from 290 to 310 K and the ambient relative humidity ranged from 7 to 17%. As shown in the figure, when the FSC is 1595 ppm, the modeling results with a fuel conversion factor of 2% matched well at low power settings, whereas the modeling results with a fuel conversion factor of 1% matched better at high power settings. When the FSC is 383 ppm, modeling results for 2% fuel conversion factor give better agreement with experimental data. This suggests that the fuel sulfur conversion factor is not a constant and can be affected by engine power settings or fuel compositions as described in the modeling work by Lukachko et al. [27]. Despite the discrepancy shown in the figure, the modeling tool is able to capture the general trend of the aerosol microphysics that take place in a near-field aircraft plume at ground level.

The particle size distributions measured during APEX reported by Lobo et al. [40] provide another way to compare our modeling data with experimental results. As shown in Fig. 12, the particle size distributions gathered during APEX at two different ambient temperatures (308.44 and 299.25 K) with highest fuel flow rate (0.84 kg/s) were compared with model predictions under 100% of engine power, 10% of ambient relative humidity, 383 ppm of FSC, and 1% of the fuel sulfur conversion factor at two different ambient temperatures (300 and 286 K). It can be seen from the figure that our model underpredicted the size of both nucleation mode and soot mode particles. These differences can be explained by the fact that our model does not include the contributions of ion-meditate and organic-enhance nucleation processes. Furthermore, the model calculations were performed under a dry condition (10% relative humidity), which minimizes the formation of nucleation mode particles. Nonetheless, the model did capture the general trend of experimental findings that lower ambient temperatures enhance the formation of nucleation mode particles significantly.

IV. Conclusions

A detailed, one-dimensional model consisting of plume chemistry, wake dilution, and aerosol microphysics was developed to study the aerosol formation dynamics in near-field aircraft plumes of CFM56-2C1 engines at ground level. Engine-exit plane conditions were obtained using a gas-turbine cycle simulation program and constrained equilibrium calculations, and plume dilution history was established using a semi-empirical approach. Aerosol microphysics was treated as a combination of H_2SO_4–H_2O binary homogeneous nucleation, volatile particle coagulation, and condensation growth on soot, and a newly developed kinetic quasi-unary nucleation theory was used. The sensitivities of the formation of sulfur-containing aerosols to ambient temperature, ambient relative humidity, engine power, and fuel sulfur content were studied for near-field aircraft plumes following the centerline trajectories up to 1 km downstream and for the APEX-1 30-m downstream sampling system.

Our simulation results at 1 km downstream show that binary homogeneous nucleation of H_2SO_4–H_2O is sensitive to ambient relative humidity and temperature. However, the condensational growth of the liquid aerosols on the soot particles is primarily dependent on engine power because the available soot surface area for condensation varies with engine power. Our results also suggest that there is a competition between the soot mode and the nucleation mode for condensable species, and this competition is most pronounced under high relative humidity and high power conditions where both processes are favored.

The calculations performed for the APEX-1 30-m sampling system demonstrate that the aerosol formation processes do not start until after the plume enters the sampling system. Similar to the 1-km plume calculations, the nucleation mode is sensitive to ambient temperature and relative humidity, and the soot mode is engine power dependent. Both the nucleation and the soot mode scale nonlinearly with fuel sulfur content. The modeling results for the 30-m sampling system described the observations in plumes with the same residence time qualitatively well. However, the particle evolution further downstream with longer residence time and higher dilution may be qualitatively and quantitatively different. This suggests that at certain ambient conditions the results gathered in the sampling system may not be representative of what would be observed in the far-field plumes.

The comparison of the experimental and modeling results shows that the modeling tool is able to capture some general trends of the aerosol microphysics. Although we only focused on one engine type in this work, the key conclusions obtained from this work, such as the sensitivity of homogeneous particle growth (nucleation mode) to the ambient temperature and relative humidity, the dependence of heterogeneous particle growth (soot mode) on the soot surface area, and the statement that particle growth observed in the 30-m downstream measurements was taking place in the sampling systems, should be general enough for other engine types. The modeling tool developed in this work can further be upgraded to help interpret experimental results and guide future experimental directions. The effects of ion-induced nucleation and organics-enhanced nucleation on the formation of aircraft-emitted aerosols that were not considered in this work will be investigated in the future.

Appendix: Davidson–Wang Semi-Empirical Algorithm for Modeling Plume Dilution

In the Davidson–Wang model, the mixing of an axisymmetric jet in a coflowing ambient fluid is divided into two regions. First, in the weakly advected, strong jet region, the centerline velocity is expressed as

$$\frac{u_{\mathrm{CL}}(x)-u_a}{u_a}=\frac{1}{\sqrt{I_m}k}\frac{\sqrt{M_{e0}}}{u_a\cdot x} \tag{A1}$$

where u_a is set nearly at zero for a grounded aircraft studied in this work, M_{e0} is calculated from the engine-exit velocities inferred from GasTurb, I_m has a value of 1.74, and k has a value of 0.107.

The centerline concentration profile in the same region is described using

$$f_{\mathrm{CL}}(x)=\frac{\sqrt{I_m}}{I_{qc}\cdot k}\frac{\sqrt{M_{e0}}}{(u_0-u_a)\cdot x} \tag{A2}$$

where I_{qc} has a value of 1.99, and u_0 is the weighted average velocity over the core and the bypass mass flow rates.

The centerline velocity and concentration profiles in the strongly advected, weak jet region are expressed as

$$\frac{u_{\mathrm{CL}}(x)-u_a}{u_a}=\left[\frac{C_{jk}^2}{9\pi k^2}\right]^{1/3}\left[\frac{\sqrt{M_{e0}}}{u_a\cdot x}\right]^{2/3} \tag{A3}$$

$$f_{\mathrm{CL}}(x)=\frac{1}{I_c}\left[\frac{C_{jk}\pi}{3k}\right]^{2/3}\left[\frac{\sqrt{M_{e0}}}{u_a\cdot x}\right]^{2/3}\left[\frac{u_a}{u_0-u_a}\right] \tag{A4}$$

in which C_{jk} has a value of 2, and I_c has a value of 4.45.

Because the Lewis number is close to unity for air, the evolution of centerline temperature as a function of downstream distance is related to the concentration dilution history described in Eqs. (A2) and (A4) by

$$\frac{T_{\mathrm{CL}}(x)-T_a}{T_0-T_a}=\frac{\sqrt{I_m}}{I_{qc}\cdot k}\frac{\sqrt{M_{e0}}}{(u_0-u_a)\cdot x} \tag{A5}$$

(weakly advected, strong jet region)

$$\frac{T_{\mathrm{CL}}(x)-T_a}{T_0-T_a}=\frac{1}{I_c}\left[\frac{C_{jk}\pi}{3k}\right]^{2/3}\left[\frac{\sqrt{M_{e0}}}{u_a\cdot x}\right]^{2/3}\left[\frac{u_a}{u_0-u_a}\right] \tag{A6}$$

(strongly advected, weak jet region)

Note that the temperature difference term in Eqs. (A5) and (A6) is weighted averaged over the core and the bypass mass flow rates. The total temperatures in Eqs. (A5) and (A6) are subsequently converted into static temperature for the microphysical simulations.

Once the centerline properties are calculated, the velocity, temperature, and exhaust gas fraction in a radial direction are described as

$$\frac{U(r,x)-U_a}{U_{\mathrm{CL}}(x)-U_a}=\frac{T(r,x)-T_a}{T_{\mathrm{CL}}(r,x)-T_a}=\frac{f(r,x)}{f_{\mathrm{CL}}(x)}=\exp\left[-\left(\frac{r}{b(x)}\right)^2\right] \tag{A7}$$

where $b(x)$ is calculated as

$$b(x)=C_L\cdot k\cdot x \qquad \text{(weakly advected, strong jet region)} \tag{A8}$$

$$b(x)=C_L\cdot\left[\frac{3k\cdot x}{C_{jk}\pi}\right]^{1/3}\left[\frac{\sqrt{M_{e0}}}{u_a}\right]^{2/3} \tag{A9}$$

(strongly advected, weak jet region)

where C_L is a constant with a value of 1 for radial velocity profiles and 1.19 for radial temperature and exhaust mass fraction profiles.

Acknowledgments

The authors are grateful for financial support from NASA through the University of Missouri–Rolla Center of Excellence for Aerospace Particulate Emission Reduction Research (Phil Whitefield, Director; NASA Cooperative Agreement NCC3-1084, Chowen Wey, Project Manager) and the Federal Aviation Administration (FAA) (under Contract/Grant No. 03-C-NE-MIT, Amendment Nos. 017 and 024, Carl Ma, Project Manager). Helpful discussions with Oluwayemisi O. Oluwole are also gratefully acknowledged.

References

[1] Waitz, I., Townsend, J., Cutcher-Gershenfeld, J., Greitzer, E., and Kerrebrock, J., "Aviation and the Environment," Report to the United States Congress, Dec. 2004.

[2] Draper, J. A., McKenny, K., Vigilante, M. L., and Wey, C. C., "Critial Issues in Aviation and the Environment 2005: Air Quality," Transportation Research Circular E-C089, Jan. 2006.

[3] Wey, C. C., Anderson, B. E., Hudgins, C., Wey, C., Li-Jones, X., Winstead, E., Thornhill, L. K., Lobo, P., Hagen, D., Whitefield, P., Yelvington, P. E., Herndon, S. C., Onasch, T. B., Miake-Lye, R. C., Wormhoudt, J., Knighton, W. B., Howard, R., Bryant, D., Corporan, E., Moses, C., Holve, D., and Dodds, W., "Aircraft Particle Emission eXperiment (APEX)," NASA TM-2006-214382, Sept. 2006.

[4] Wey, C. C., Anderson, B. E., Wey, C., Miake-Lye, R. C., Whitefield, P., and Howard, R., "Overview on the Aircraft Particle Emissions eXperiment," *Journal of Propulsion and Power*, Vol. 23, No. 5, 2007, pp. 898–905.
doi:10.2514/1.26406

[5] Miake-Lye, R. C., Brown, R. C., Anderson, M. R., and Kolb, C. E., "Calculations of Condensation and Chemistry in an Aircraft Contrail," DLR-Mitteilung Paper 94-06, April 1994.

[6] Brown, R. C., Miake-Lye, R. C., Anderson, M. R., Kolb, C. E., and Resch, T. J., "Aerosol Dynamics in Near-Field Aircraft Plumes," *Journal of Geophysical Research*, Vol. 101, No. D17, 1996, pp. 22939–22953.
doi:10.1029/96JD01918

[7] Brown, R. C., Anderson, M. R., Miake-Lye, R. C., Kolb, C. E., Sorokin, A. A., and Buriko, Y. Y., "Aircraft Exhaust Sulfur Emissions," *Geophysical Research Letters*, Vol. 23, No. 24, 1996, pp. 3603–3606.
doi:10.1029/96GL03339

[8] Brown, R. C., Miake-Lye, R. C., Anderson, M. R., and Kolb, C. E., "Effect of Aircraft Exhaust Sulfur Emissions on Near Field Plume Aerosols," *Geophysical Research Letters*, Vol. 23, No. 24, 1996, pp. 3607–3610.
doi:10.1029/96GL03338

[9] Yu, F., and Turco, R. P., "The Role of Ions in the Formation and Evolution of Particles in Aircraft Plumes," *Geophysical Research Letters*, Vol. 24, No. 15, 1997, pp. 1927–1930.
doi:10.1029/97GL01822

[10] Yu, F., and Turco, R. P., "Evolution of Aircraft-Generated Volatile Particles in the Far Wake Regime: Potential Contributions to Ambient CCN/IN," *Geophysical Research Letters*, Vol. 26, No. 12, 1999, pp. 1703–1706.
doi:10.1029/1999GL900324

[11] Kärcher, B., "Physicochemistry of Aircraft-Generated Liquid Aerosols, Soot, and Ice Particles 1. Model Description," *Journal of Geophysical Research*, Vol. 103, No. D14, 1998, pp. 17111–17128.
doi:10.1029/98JD01044

[12] Kärcher, B., "On the Potential Importance of Sulfur-Induced Activation of Soot Particles in Nascent Jet Aircraft Exhaust Plumes," *Atmospheric Research*, Vol. 46, Nos. 3–4, 1998, pp. 293–305.
doi:10.1016/S0169-8095(97)00070-7

[13] Kärcher, B., Turco, R. P., Yu, F., Danilin, M. Y., Weisenstein, D. K., Miake-Lye, R. C., and Busen, R., "A Unified Model for Ultrafine Aircraft Particle Emissions," *Journal of Geophysical Research*, Vol. 105, No. D24, 2000, pp. 29379–29386.
doi:10.1029/2000JD900531

[14] Andronache, C., and Chameides, W. L., "Interactions Between Sulfur and Soot Emissions from Aircraft and Their Role in Contrail Formation: 2. Development," *Journal of Geophysical Research*, Vol. 103, No. D9, 1998, pp. 10787–10802.
doi:10.1029/98JD00173

[15] Gleitsmann, G., and Zellner, R., "A Modeling Study of the Formation of Cloud Condensation Nuclei in the Jet Regime of Aircraft Plumes," *Journal of Geophysical Research*, Vol. 103, No. D16, 1998, pp. 19543–19555.
doi:10.1029/98JD01733

[16] Gleitsmann, G., and Zellner, R., "The Effects of Ambient Temperature and Relative Humidity on Particle Formation in the Jet Regime of Commercial Aircraft: A Modeling Study," *Atmospheric Environment*, Vol. 32, No. 18, 1998, pp. 3079–3087.
doi:10.1016/S1352-2310(98)00062-4

[17] Yu, F., "Chemiions and Nanoparticle Formation in Diesel Engine Exhaust," *Geophysical Research Letters*, Vol. 28, No. 22, 2001, pp. 4191–4194.
doi:10.1029/2001GL013732

[18] Yu, F., "Chemiion Evolution in Motor Vehicle Exhaust: Further Evidence of Its Role in Nanoparticle Formation," *Geophysical Research Letters*, Vol. 29, No. 15, 2002, pp. 12/1–12/4.
doi: 10.1029/2002GL015004

[19] Zhang, K. M., and Wexler, A. S., "Evolution of Particle Number Distribution Near Roadways. Part 1: Analysis of Aerosol Dynamics and Its Implications for Engine Emission Measurement," *Atmospheric Environment*, Vol. 38, No. 38, 2004, pp. 6643–6653.
doi:10.1016/j.atmosenv.2004.06.043

[20] Zhang, K. M., Wexler, A. S., Zhu, Y. F., and Hinds, W. C., "Evolution of Particle Number Distribution Near Roadways. Part 2: The 'Road-to-Ambient' Process," *Atmospheric Environment*, Vol. 38, No. 38, 2004, pp. 6655–6665.
doi:10.1016/j.atmosenv.2004.06.044

[21] Zhang, K. M., Wexler, A. S., Niemeier, D. A., Zhu, Y. F., Hinds, W. C., and Sioutas, C., "Evolution of Particle Number Distribution Near Roadways. Part 3: Traffic Analysis and On-Road Size Resolved Particulate Emission Factors," *Atmospheric Environment*, Vol. 39, No. 22, 2005, pp. 4155–4166.
doi:10.1016/j.atmosenv.2005.04.003

[22] Du, H., and Yu, F., "Role of the Binary H_2SO_4-H_2O Homogeneous Nucleation in the Formation of Volatile Nanoparticles in the Vehicular Exhaust," *Atmospheric Environment*, Vol. 40, No. 39, 2006, pp. 7579–7588.
doi:10.1016/j.atmosenv.2006.07.012

[23] Vancassel, X., Sorokin, A., Mirabel, P., Petzold, A., and Wilson, C., "Volatile Particles Formation During PartEmis: A Modeling Study," *Atmospheric Chemistry and Physics*, Vol. 4, No. 2, 2004, pp. 439–447.

[24] Kurzke, J., *GasTurb 10: A Program for Gas-Turbine Performance Calculations*, Dr. Joachim Kurzke, Dachau, Germany, 2004.

[25] Lambert, M., *Jane's All the World's Aircraft 1993–1994*, Jane's Information Group Ltd., London, U.K., 1993.

[26] International Civil Aviation Organization, "ICAO Engine Emission Databank," DOC 9646-AN/943, 1995.

[27] Lukachko, S. P., Waitz, I. A., Miake-Lye, R. C., and Brown, R. C., "Engine Design and Operational Impacts on Particulate Matter Precursor Emissions," ASME Paper GT2005-69112, June 2005.

[28] Davidson, M. J., and Wang, H. J., "Strongly Advected Jet in a Coflow," *Journal of Hydraulic Engineering*, Vol. 128, No. 8, 2002, pp. 742–752.
doi:10.1061/(ASCE)0733-9429(2002)128:8(742)

[29] Mueller, M. A., Yetter, R. A., and Dryer, F. L., "Kinetic Modeling of the $CO/H_2O/O_2/NO/SO_2$ System: Implications for High-Pressure Fall-Off in the $SO_2 + O(+M) = SO_3(+M)$ Reaction," *International Journal of Chemical Kinetics*, Vol. 32, No. 6, 2000, pp. 317–339.
doi:10.1002/(SICI)1097-4601(2000)32:6<317::AID-KIN1>3.0.CO;2-L

[30] Lee, R. J., Rupley, F. M., and Miller, J. A., *CHEMKIN-III: A Fortran Chemical Kinetics Package for the Analysis of Gas-Phase Chemical and Plasma Kinetics*, Reaction Design, San Diego, CA, 1996.

[31] Yu, F., "Quasi-Unary Homogeneous Nucleation of H_2SO_4-H_2O," *Journal of Chemical Physics*, Vol. 122, No. 7, 2005, pp. 074501/1–074501/8.
doi:10.1063/1.1850472

[32] Yu, F., "Binary H_2SO_4-H_2O Homogeneous Nucleation Based on Kinetic Quasi-Unary Nucleation Model: Look-Up Tables," *Journal of Geophysical Research*, Vol. 111, No. D4, 2006, pp. D04201/1–D04201/17.
doi:10.1029/2005JD006358

[33] Seinfeld, J. H., and Pandis, S. N., *Atmospheric Chemistry and Physics—from Air Pollution to Climate Change*, Wiley, New York, 1998.

[34] Fuchs, N. A., *The Mechanics of Aerosols*, Dover, New York, 1989.

[35] Jacobson, M. Z., and Turco, R. P., "Simulating Condensational Growth, Evaporation, and Coagulation of Aerosols Using a Combined Moving and Stationary Size Grid," *Aerosol Science and Technology*, Vol. 22, No. 1, 1995, pp. 73–92.
doi:10.1080/02786829408959729

[36] Zhang, D., and Zhang, R., "Laboratory Investigation of Heterogeneous Interaction of Sulfuric Acid with Soot," *Environmental Science and Technology*, Vol. 39, No. 15, 2005, pp. 5722–5728.
doi:10.1021/es050372d

[37] Pruppacher, H. R., and Klett, J. D., *Microphysics of Clouds and Precipitation*, 2nd ed., Kluwer Academic Publishers, Dordrecht, The Netherlands, 1997.

[38] Schumann, U., Arnold, F., Busen, R., Curtius, J., Kärcher, B., Kiendler, A., Petzold, A., Schlager, H., Schroder, F., and Wohlfrom, K.-H., "Influence of Fuel Sulfur on the Composition of Aircraft Exhaust Plumes: The Experiments SULFUR 1–7," *Journal of Geophysical Research*, Vol. 107, No. D15, 2002, pp. 4247–4273.
doi:10.1029/2001JD000813

[39] Anderson, B. E., Winstead, E. L., Hudgins, C. H., and Thornhill, K. L., "Concentrations and Physical Properties of Particles Within the Exhaust of a CFM-56 Engine," NASA TM-2006-214382, Appendix H, Sept. 2006.

[40] Lobo, P., Hagen, D. E., Whitefield, P. D., and Alofs, D. J., "Physical Characterization of Aerosol Emissions from a Commercial Gas Turbine Engine," *Journal of Propulsion and Power*, Vol. 23, No. 5, 2007, pp. 919–929.
doi:10.2514/1.26772

[41] Arnold, F., Kiendler, A., Wiedemer, V., Aberle, S., and Stilp, T., "Chemiion Concentration Measurements in Jet Engine Exhaust at the Ground: Implications for Ion Chemistry and Aerosol Formation in the Wake of a Jet Aircraft," *Geophysical Research Letters*, Vol. 27, No. 12, 2000, pp. 1723–1726.
doi:10.1029/1999GL011096

[42] Eichkorn, S., Wohlfrom, K.-H., Arnold, F., and Busen, R., "Massive Positive and Negative Chemiions in the Exhaust of an Aircraft Jet Engine at Ground Level: Mass Distribution Measurements and

Implications for Aerosol Formation," *Atmospheric Environment*, Vol. 36, No. 11, 2002, pp. 1821–1825.
doi:10.1016/S1352-2310(02)00142-5

[43] Kiendler, A., and Arnold, F., "Unambiguous Identification and Measurement of Sulfuric Acid Cluster Chemiions in Aircraft Jet Engine Exhaust," *Atmospheric Environment*, Vol. 36, No. 11, 2002, pp. 1757–1761.
doi:10.1016/S1352-2310(02)00154-1

[44] Haverkamp, H., Wilhelm, S., Sorokin, A., and Arnold, F., "Positive and Negative Ion Measurements in Jet Aircraft Engine Exhaust: Concentrations, Sizes and Implications for Aerosol Formation," *Atmospheric Environment*, Vol. 38, No. 18, 2004, pp. 2879–2884.
doi:10.1016/j.atmosenv.2004.02.028

[45] Miller, T. M., Ballenthin, J. O., Viggiano, A. A., Anderson, B. E., and Wey, C. C., "Mass Distribution and Concentrations of Negative Chemiions in the Exhaust of a Jet Engine: Sulfuric Acid Concentrations and Observation of Particle Growth," *Atmospheric Environment*, Vol. 39, No. 17, 2005, pp. 3069–3079.
doi:10.1016/j.atmosenv.2005.01.034

[46] Yu, F., "From Molecular Clusters to Nanoparticles: Second-Generation Ion-Mediated Nucleation Model," *Atmospheric Chemistry and Physics*, Vol. 6, No. 12, 2006, pp. 5193–5211.

[47] Yu, F., "Modified Kelvin-Thomson Equation Considering Ion-Dipole Interaction: Comparison with Observed Ion-Clustering Enthalpies and Entropies," *Journal of Chemical Physics*, Vol. 122, No. 8, 2005, pp. 084503/1–084503/8.
doi:10.1063/1.1845395

[48] Zhang, R., Suh, I., Zhao, J., Zhang, D., Fortner, E. C., Tie, X., Molina, L. T., and Molina, M. J., "Atmospheric New Particle Formation Enhanced by Organic Acids," *Science*, Vol. 304, No. 5676, 2004, pp. 1487–1490.
doi:10.1126/science.1095139

[49] Knighton, W. B., Rogers, T. M., Anderson, B. E., Herndon, S. C., Yelvington, P. E., and Miake-Lye, R. C., "Quantification of Aircraft Engine Hydrocarbon Emissions Using Proton Transfer Reaction Mass Spectrometry," *Journal of Propulsion and Power*, Vol. 23, No. 5, 2007, pp. 949–958.
doi:10.2514/1.22965

[50] Yelvington, P. E., Herndon, S. C., Wormhoudt, J. C., Jayne, J. T., Miake-Lye, R. C., Knighton, W. B., and Wey, C., "Chemical Speciation of Hydrocarbon Emissions from a Commercial Aircraft Engine," *Journal of Propulsion and Power*, Vol. 23, No. 5, 2007, pp. 912–918.
doi:10.2514/1.23520

[51] Onasch, T. B., Jayne, J. T., Herndon, S. C., Mortimer, P., Worsnop, D. R., and Miake-Lye, R. C., "Chemical Properties of Aircraft Engine Exhaust Aerosols Sampled During APEX," NASA TM-2006-214382, Appendix J, Sept. 2006.

L. Maurice
Associate Editor